Available online at www.sciencedirect.com
ScienceDirect
Acta Materialia 54 (2006) 4781–4792
Acta MATERIALIA
www.actamat-journals.com

Uniaxial tensile plastic deformation and grain growth of bulk nanocrystalline alloys

G.J. Fan [a,*], L.F. Fu [b], H. Choo [a,c], P.K. Liaw [a], N.D. Browning [b,d]

[a] Department of Materials Science and Engineering, University of Tennessee, Knoxville, TN 37996, USA
[b] Department of Chemical Engineering and Materials Science, University of California, Davis, CA 95616, USA
[c] Metals and Ceramic Division, Oak Ridge National Laboratory, Oak, Ridge, TN 37831, USA
[d] National Center for Electron Microscopy, Lawrence Berkeley National Laboratory, Berkeley, CA 94720, USA

Received 15 February 2006; received in revised form 21 May 2006; accepted 7 June 2006
Available online 11 September 2006

Abstract

The uniaxial tensile behavior of as-deposited bulk nanocrystalline (nc) Ni–Fe (average grain size $d \approx 23$ nm) and Co–P ($d \approx 12$ nm) alloys was investigated. Both alloys have a high strength of about 2 GPa. The nc Ni–Fe alloy exhibits a tensile elongation to failure, ε_f, in the range 4–7%, depending on the applied strain rate, $\dot{\varepsilon}$. In contrast, the nc Co–P alloy shows rather constant ε_f of about 2.2%, which is insensitive to $\dot{\varepsilon}$. Tensile plastic deformation causes a grain growth in both alloys. An abnormal grain growth was noticed in the nc Ni–Fe alloy, leading to a bimodal microstructure with large grain sizes up to about 250 nm. While deformation twinning and dislocation motion still play roles, our experimental results indicate that the plastic deformation of the nc alloys is influenced by the grain boundary activities.

Keywords: Nanocrystalline alloys; Mechanical properties; Grain growth; Deformation mechanisms

1. Introduction

Nanocrystalline (nc) metals and alloys, with grain sizes typically ranging from 2 to 100 nm, have received worldwide attention, due to the new deformation mechanisms not yet fully explored as well as the extraordinarily high strengths suitable for potentially new engineering applications [1–10]. For conventional metals and alloys, plastic deformation occurs by dislocation activities. When the grain size is reduced to the nanometer range, dislocation nucleation from the Frank–Read source within the grains may become difficult [11]. Therefore, much effort has been made to understand deformation mechanisms of nc materials, in particular for metals and alloys with average grain sizes less than 30 nm [3,4,8–25]. Grain boundary (GB)-accommodated deformation, rather than the dislocation pileup mechanism, was suggested to be the dominant deformation mechanism for nc materials with very fine grain sizes [11–13,20–22], although dislocation activities may still be operative [8,17–19,23–25]. GB-accommodated deformation for nc materials has been reported in very thin-film samples with a thickness of several tens of nanometers [20,26]. Due to the lack of the three-dimensional constraint and a high volume fraction of the surface, two-dimensional thin-film samples may not represent the mechanical behavior of bulk polycrystalline samples [27]. GB-accommodated deformation would impart a reasonable tensile ductility to nc materials. However, the available experimental evidence indicates that nc materials with a thickness of several tens of micrometers often show very little tensile ductility [14,28], suggesting that the GB-accommodated deformation is unlikely to be the dominant mechanism for these materials. The tensile ductility of nc materials is often reduced when large tensile specimens are tested [2,4,14].

* Corresponding author.
E-mail address: gfan@utk.edu (G.J. Fan).

1359-6454/$30.00
doi:10.1016/j.actamat.2006.06.016

The low tensile ductility of nc metals and alloys has been attributed either to extrinsic factors, such as porosity and/or second-particle inclusions, or to intrinsic factors, such as the lack of hardening during the plastic deformation of nc materials [27,29]. Therefore, extensive efforts were made previously to improve the tensile ductility of bulk nc metals by employing various toughening strategies [27,29], including the introduction of a heterogeneous microstructure with a bimodal grain size distribution across different length scales [7,30–32]. In the case of bimodal ultrafine-grained (UFG)/nc metals and alloys, dislocation motions together with shear-band localization and deformation twinning are mainly responsible for the plastic deformation [7,30–32]. Good tensile ductility, combined with a high strength, was realized in bulk nc pure copper prepared by severe plastic deformation [33]. The as-prepared bulk nc copper exhibits a narrow grain size distribution. However, in situ transmission electron microscopy (TEM) observations indicated that the plastic deformation of the nc copper was mainly mediated by the dislocation motions, as evidenced by the dislocation pileups at the GBs.

Recent reports [34–36] indicate that some face-centered cubic (fcc) nc alloys prepared by electrodeposition exhibit good ductility, which may be due to the increase in the strain hardening rate by adding the alloying elements. In this article, the uniaxial tensile behavior of bulk nc Ni–Fe and nc Co–P alloys prepared by electrodeposition is discussed. In contrast to the nc Co–P alloy, which exhibits high strength with relatively low tensile ductility, a combination of high strength and good tensile ductility was obtained for the nc Ni–Fe alloy. By varying the specimen sizes and the strain rates, we report that the mechanical properties of the nc Ni–Fe and nc Co–P alloys exhibit various size- and strain-rate dependences.

It is well known that nc metals and alloys will undergo grain growth during thermal annealing to reduce the grain boundary areas [37]. Recent studies indicate that grain growth occurs in nc metals under various stress modes, including nanoindentation [38–41], high-pressure torsion [42], uniaxial tension [43–45] and uniaxial compression [46]. For example, rapid grain growth was induced by nanoindentation in nc Cu and Al near the indenter tip with high stress concentration [38–41]. In this paper, we report that the grains grow in the nc Ni–Fe and Co–P alloys during uniaxial tensile plastic deformation. Evidence of the abnormal grain growth during plastic deformation of the nc Ni–Fe alloy is presented. Finally, the underlying deformation mechanisms of the nc alloys are discussed.

2. Experimental

Bulk nc Ni–18 wt.% Fe and nc Co–1.65 wt.% P alloy sheets were produced using a pulsed electrodeposition technique by Integran Technologies Inc. [47]. The crystal structure of the as-deposited samples was determined using X-ray diffraction (XRD). The as-deposited alloy sheets had dimensions of 70 mm × 70 mm × 3 mm (nc Ni–Fe alloy) and 70 mm × 10 mm × 2.5 mm (nc Co–P alloy). Dog-bone specimens were machined from the as-deposited sheets with various gauge cross sections and gauge lengths (see Table 1), and were polished for the uniaxial tensile tests. An extensometer was used during the tests for precise strain measurements. The fracture surfaces were examined using scanning electron microscopy (SEM). TEM and high-resolution TEM (HRTEM) observations were carried out before and after tensile plastic deformation, using a Schottky field-emission gun FEI Tecnai F20 UT microscope operating at 200 kV with a spatial resolution of 0.14 nm. Due to the occurrence of necking instability, the tensile plastic deformation often causes a large local plastic strain close to the fractured surface. Therefore, the TEM and HRTEM specimens were cut from places away from the fractured surface to ensure that the microstructure changes observed by TEM and HRTEM were due to homogeneous plastic deformation. TEM and HRTEM thin-foil specimens were prepared by the conventional twin-jet electropolishing technique using a 25% nitric acid +75% methanol solution at −30 °C and 10 V for the nc Ni–Fe alloy and a 23% perchloric acid and 77% acetic acid electrolyte at 18 °C and 12 V for the nc Co–P alloy.

3. Results

3.1. Microstructures

The XRD patterns of the as-deposited bulk nc Ni–Fe and nc Co–P alloys show a single-phase supersaturated solid solution with a fcc structure for both alloys (Fig. 1). No additional phases were noticed in the XRD patterns. The metastable fcc structure of the nc Ni–Fe alloy is in good agreement with previous reports [48,49]. However, a hexagonal close-packed (hcp) structure was reported for as-deposited nc pure Co metal by Karimpoor et al. [47]. The hcp structure was also reported by Choi et al. [50] in an as-deposited nc Co–1.1 at.% P alloy. These results are contrary to those for the present bulk nc Co–P alloy, which shows a fcc structure.

The microstructures of the as-deposited nc Ni–Fe and Co–P alloys were examined using TEM and HRTEM. The TEM images taken from the area close to the substrate and the area from the upper growth surface indicate that the grain sizes are fairly uniform for the nc Ni–Fe and Co–P alloys along the deposition growth direction. However, the grain sizes are about twice as large along the deposition growth direction as those perpendicular to the deposition growth direction, indicating a columnar structure for nc Ni–Fe and Co–P alloys. Fig. 2 shows bright-field TEM and HRTEM images for the as-deposited nc Ni–Fe alloy perpendicular to the deposition growth direction. The average grain size of the nc Ni–Fe alloy (Fig. 2(a)) is about 23 nm. Further HRTEM observations indicate that the neighboring grains are separated by high-angle GBs. Samples prepared by the electrodeposition method often contain a certain amount of twins [15,51]. In

Table 1
Mechanical properties (plastic strain at UTS, ε_{UTS}; total plastic strain, ε_p; tensile elongation to failure, ε_f; UTS; fracture strength, σ_f) of the bulk nc Ni–Fe and nc Co–P alloys with various gauge dimensions (length × width × thickness) measured from tensile tests at $\dot{\varepsilon} = 10^{-3}$ s^{-1}

Gauge dimensions (mm)	ε_{UTS} (%)	ε_p (%)	ε_f (%)	UTS (MPa)	σ_f (MPa)
12 × 1 × 0.5 (nc Ni–Fe)	5.1 ± 0.3	6.0 ± 0.3	6.7 ± 0.3	1990 ± 70	1930 ± 70
18 × 2 × 1 (nc Ni–Fe); Sample I	5.0 ± 0.3	5.7 ± 0.3	6.4 ± 0.3	1990 ± 60	1930 ± 70
25 × 4 × 1 (nc Ni–Fe)	5.1 ± 0.4	5.9 ± 0.4	6.6 ± 0.4	1990 ± 60	1950 ± 50
25 × 4 × 3 (nc Ni–Fe)	5.0 ± 0.4	5.6 ± 0.4	6.3 ± 0.4	1980 ± 70	1940 ± 70
15 × 1.5 × 0.5 (nc Co–P); Sample II	1.4 ± 0.2	1.7 ± 0.2	2.3 ± 0.2	1970 ± 80	1950 ± 80
30 × 3 × 0.8 (nc Co–P)	0.3 ± 0.1	0.3 ± 0.1	1.0 ± 0.1	1600 ± 80	1600 ± 80
30 × 3 × 2 (nc Co–P)	0	0	0.4 ± 0.1	1070 ± 150	1070 ± 150

For each gauge dimension, three tensile specimens were tested.

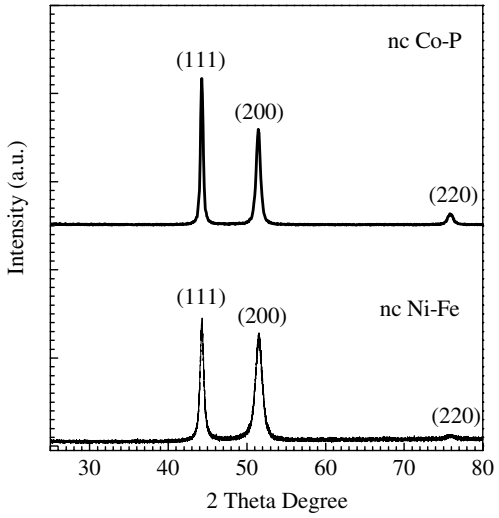

Fig. 1. XRD patterns of the as-deposited bulk nc Ni–Fe and nc Co–P alloys showing the single-phase fcc structure for both alloys in the as-deposited state.

the case of the nc Ni–Fe alloy, growth twins were not observed in the HRTEM images. Instead, dislocations were observed in the as-deposited sample. A typical example of growth dislocations is shown in Fig. 2(b).

The microstructures of the as-deposited nc Co–P alloy perpendicular to the deposition growth direction are shown in Fig. 3. The as-deposited nc Co–P alloy has an average grain size of about 12 nm. These grains contain a high density of nanotwins [47], which were attributed to the low stacking fault energy of Co metal [47]. The spacing of twin lamellae is 1–2 nm (Fig. 3(b)).

3.2. Specimen size effects on the mechanical properties

It was reported that nc metals often exhibit a size effect, i.e., the tensile elongation to failure and the fracture strength decrease with increasing gauge dimensions of the tensile specimens [2,4,14]. The reported size effects on the mechanical properties were attributed to the presence of the artifacts, such as the porosity and/or second-phase particle inclusions, in the nc specimens [27,29]. The size effects on the mechanical properties of the bulk nc Ni–Fe and nc Co–P alloys were investigated by varying the gauge lengths and gauge cross sections of the tensile specimens. Fig. 4 shows a typical dog-bone specimen with an initial gauge length of 18 mm and gauge cross section of 2 mm × 1 mm for the nc Ni–Fe alloy before and after the tensile plastic deformation. The corresponding engineering stress–strain curve is shown in Fig. 5. The engineering stress–strain

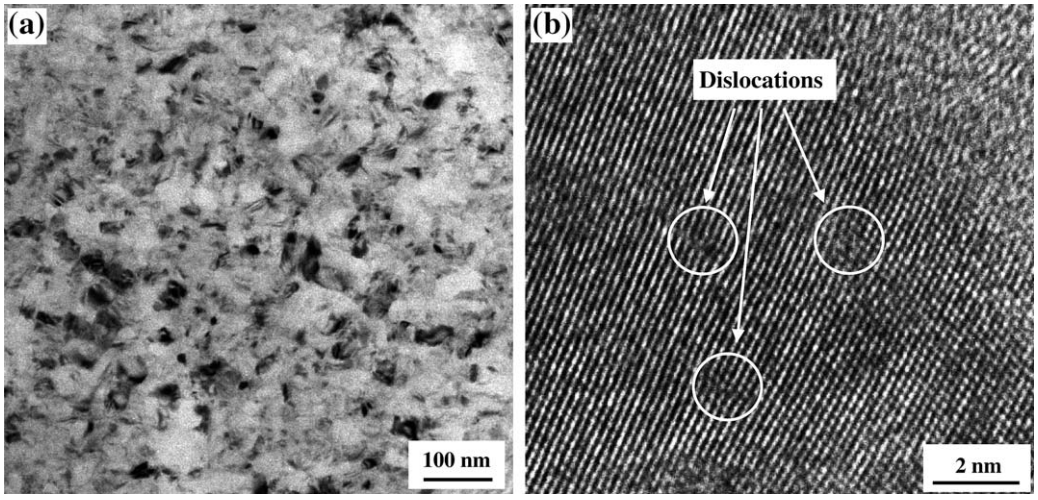

Fig. 2. Bright-field TEM image (a) and the HRTEM image (b) of the as-deposited bulk nc Ni–Fe alloy perpendicular to the deposition growth direction. The average grain size of the as-deposited nc Ni–Fe alloy is about 23 nm (a). The as-deposited sample contains the growth dislocations (b).

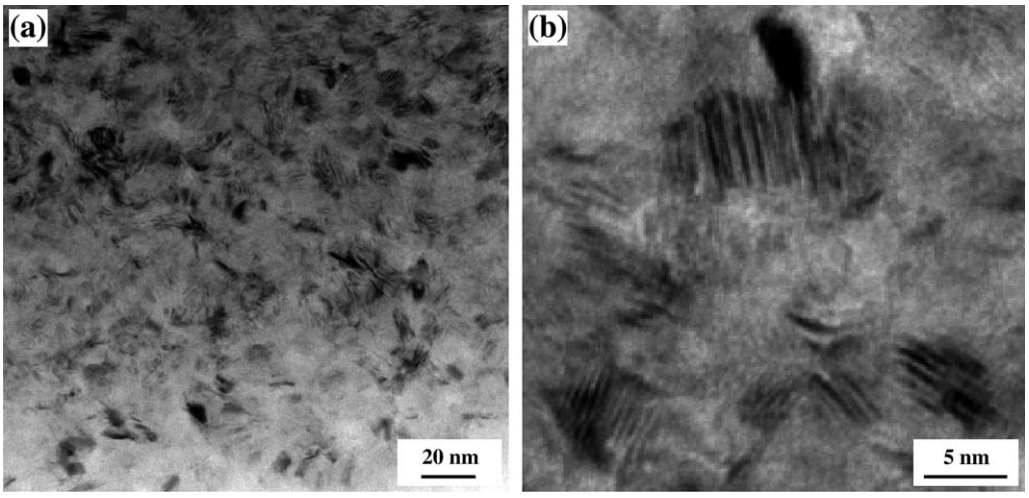

Fig. 3. Bright-field TEM image of the as-deposited bulk nc Co–P alloy perpendicular to the deposition growth direction, showing the average grain size of about 12 nm (a). The as-deposited nc Co–P alloy contains a high density of growth twins. The high-magnification image (b) indicates that the spacing of the twin lamellae is about 1 nm.

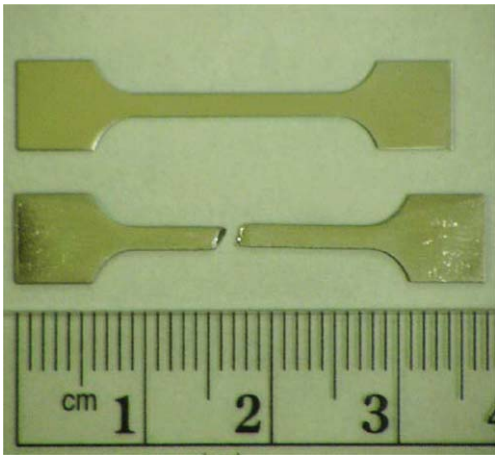

Fig. 4. A dog-bone specimen with the initial gauge dimensions of 18 mm × 2 mm × 1 mm for the bulk nc Ni–Fe alloy before and after the tensile test.

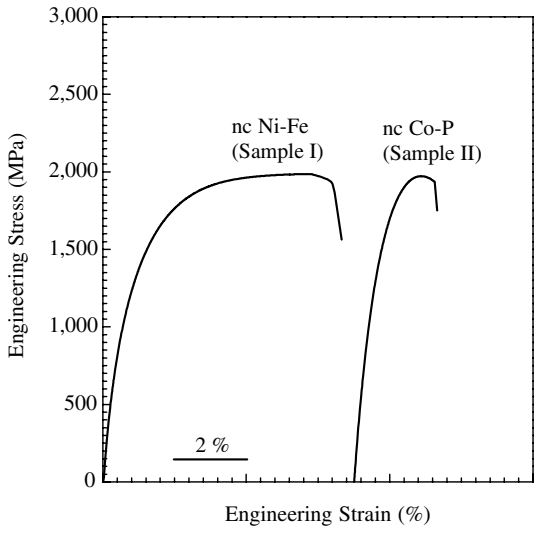

Fig. 5. Engineering stress–strain curves of the bulk nc Ni–Fe (Sample I: 18 mm × 2 mm × 1 mm) and nc Co–P alloys (Sample II: 15 mm × 1.5 mm × 0.5 mm) measured during the tensile tests at a strain rate, $\dot{\varepsilon}$, of 10^{-3} s^{-1}.

curve for the nc Co–P alloy with the initial gauge length of 15 mm and gauge cross section of 1.5 mm × 0.5 mm is also included in Fig. 5. It was determined that the nc Ni–Fe alloy has a plastic strain at the ultimate tensile strength (UTS), ε_{UTS}, a plastic strain, ε_p, a tensile elongation to failure, ε_f; UTS and a fracture strength, σ_f, of 5.0%, 5.7%, 6.4%, 1990 MPa and 1930 MPa, respectively; the nc Co–P alloy exhibits comparable values of UTS and σ_f of about 1970 MPa and 1950 MPa, but smaller values of ε_{UTS}, ε_p and ε_f of about 1.4%, 1.7% and 2.3%, respectively.

Table 1 summarizes the mechanical properties of the nc Ni–Fe and nc Co–P alloys as a function of gauge dimensions at a strain rate, $\dot{\varepsilon}$, of 10^{-3} s^{-1}. Contrary to the previous reports [2,4,14], the mechanical properties of the nc Ni–Fe alloys did not exhibit a clear size effect. On steadily increasing the gauge dimensions from 12 mm × 1 mm × 0.5 mm to 25 mm × 4 mm × 3 mm, ε_{UTS}, ε_p, ε_f, UTS and σ_f exhibit similar values of 5.0%, 5.8%, 6.5%, 1990 MPa and 1940 MPa, respectively. In contrast, the nc Co–P alloy demonstrated a strong size effect. On increasing the gauge dimensions from 15 mm × 1.5 mm × 0.5 mm to 30 mm × 3 mm × 2 mm, ε_p was completely lost from 1.7%, while σ_f decreased sharply from 1950 to 1070 MPa. The above results indicate that that the nc Co–P alloy had artifacts in the as-deposited state unlike the nc Ni–Fe alloy, which is consistent with the relatively brittle behavior of the nc Co–P alloy with a low value of ε_f.

3.3. Strain rate effects on the plastic flow

To understand the strain rate effects on the plastic flow of the nc Ni–Fe and nc Co–P alloys, the nc Ni–Fe alloy

with the gauge dimension of 18 mm × 2 mm × 1 mm (denoted as Sample I in Table 1) and nc Co–P alloy with the gauge dimension of 15 mm × 1.5 mm × 0.5 mm (denoted as Sample II) were subjected to a further investigation. Fig. 6 shows a few examples of the engineering stress–strain curves of the nc Ni–Fe and Co–P alloys measured as a function of $\dot{\varepsilon}$ that ranges from 10^{-5} to 10 s^{-1}. For both nc alloys, the UTS increases slightly with increasing $\dot{\varepsilon}$, indicating a very small value of the strain rate sensitivity, m, which was defined by

$$m = \left.\frac{\partial \log \sigma}{\partial \log \dot{\varepsilon}}\right|_{\varepsilon,T} \quad (1)$$

where σ is the tensile stress at a constant strain, ε, and temperature, T. The relationship between σ at $\varepsilon = 2\%$ and $\dot{\varepsilon}$ at room temperature is plotted in Fig. 7(a). The m values were determined to be 0.0052 and 0.0014 for the nc Ni–Fe and nc Co–P alloy, respectively.

From Fig. 6, it is also noticed that the plasticity of the nc Ni–Fe alloy exhibits a strong rate sensitivity, while the plasticity of the nc Co–P alloy was not affected by the applied $\dot{\varepsilon}$. The quantitative relationship between ε_f and $\dot{\varepsilon}$ is plotted in Fig. 7(b). It is noted that ε_f of the nc Ni–Fe alloy increases continuously from 4.4 to 7.4% on increasing $\dot{\varepsilon}$ from 10^{-5} to 10^{-1} s^{-1}, and drops to 5.1% on further increasing $\dot{\varepsilon}$ to 10 s^{-1}. However, ε_f of the nc Co–P alloy remains constant at 2.2% when $\dot{\varepsilon}$ changes from 10^{-5} to 10 s^{-1}.

Fig. 8 shows SEM images of the fracture surfaces of the nc Ni–Fe alloy deformed at $\dot{\varepsilon} = 10^{-3}$ s^{-1} to $\varepsilon_f = 6.4\%$, and the nc Co–P alloy deformed at $\dot{\varepsilon} = 10^{-3}$ s^{-1} to $\varepsilon_f = 2.3\%$. Shear bands were often observed during the plastic deformation of nc metals and alloys [31,32,52]. In the case of nc Ni–Fe and Co–P alloys, shear bands were not observed using SEM in the side surfaces of the fractured specimens. Both nc alloys show a dimpled structure with a dimple size several times larger than the initial grain sizes in the as-deposited state, in agreement with previous reports [53,54]. Compared with the nc Co–P alloy, the nc Ni–Fe alloy appears more ductile due to: (a) necking (Fig. 8(a)), which was clearly observed from SEM during the plastic deformation with some post-necking deformation (Fig. 5(a)); (b) cracks observed on the side surfaces of the fractured nc Co–P specimens (Fig. 8(c)); and (c) the relatively rough fracture surface of the nc Ni–Fe alloy, which is an indication of the extensive plastic deformation prior to fracture.

3.4. Grain growth induced by tensile plastic deformation

To reveal the microstructural changes caused by tensile plastic deformation, the microstructures of the nc Ni–Fe and nc Co–P alloys after the plastic deformation were further examined using TEM and HRTEM. Fig. 9 shows the bright-field TEM images of the nc Ni–Fe alloy deformed at $\dot{\varepsilon} = 10^{-3}$ s^{-1} to $\varepsilon_f = 4.0$ and to 6.4%. Compared to Fig. 2 of the as-deposited alloy, a substantial grain growth was observed after the tensile plastic deformation. The average grain size increases from 23 nm in the as-deposited state to approximately 40 nm at $\varepsilon_f = 4.0\%$ (Fig. 9(a)), and to approximately 61 nm at $\varepsilon_f = 6.4\%$ (Fig. 9(b)). Moreover, several grains larger than 200 nm are observed in Fig. 9(b), indicating that the abnormal grain growth occurred during the plastic deformation. The abnormal grain growth was more clearly evidenced in the grain size distribution statistics shown in Fig. 10. The as-deposited nc Ni–Fe alloy exhibits a relatively narrow grain size distribution (Fig. 10(a)). After the plastic deformation to $\varepsilon_f = 6.4\%$ (Fig. 10(b)), the grain size distribution became much wider. Most importantly, due to the abnormal grain

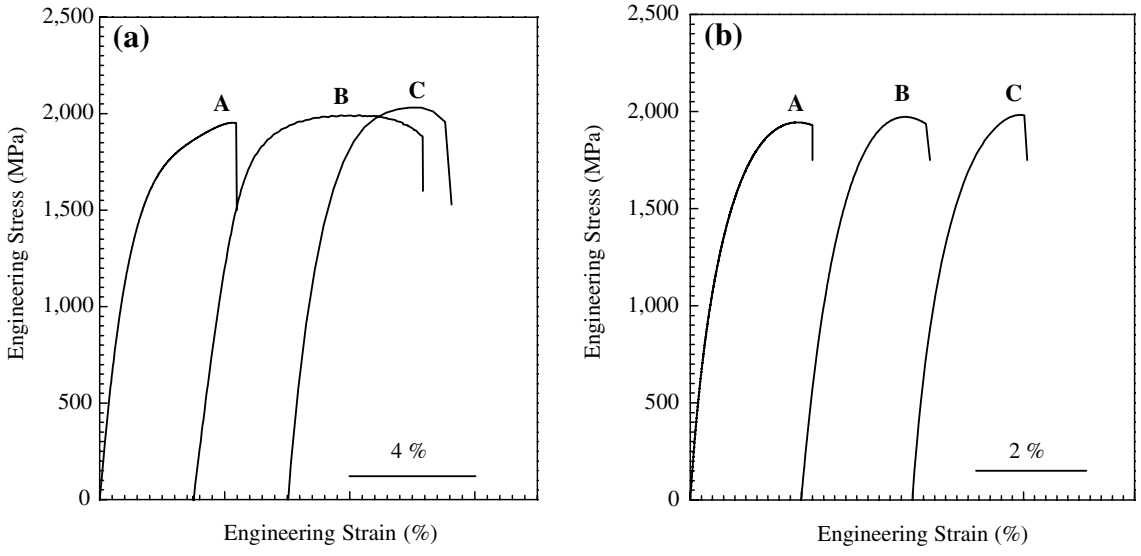

Fig. 6. Examples of the engineering stress–strain curves of the bulk nc Ni–Fe alloy (a) and bulk nc Co–P alloy (b) measured during tensile deformation at various strain rates (A: $\dot{\varepsilon} = 10^{-5}$ s^{-1}; B: $\dot{\varepsilon} = 10^{-2}$ s^{-1}; C: $\dot{\varepsilon} = 10$ s^{-1}).

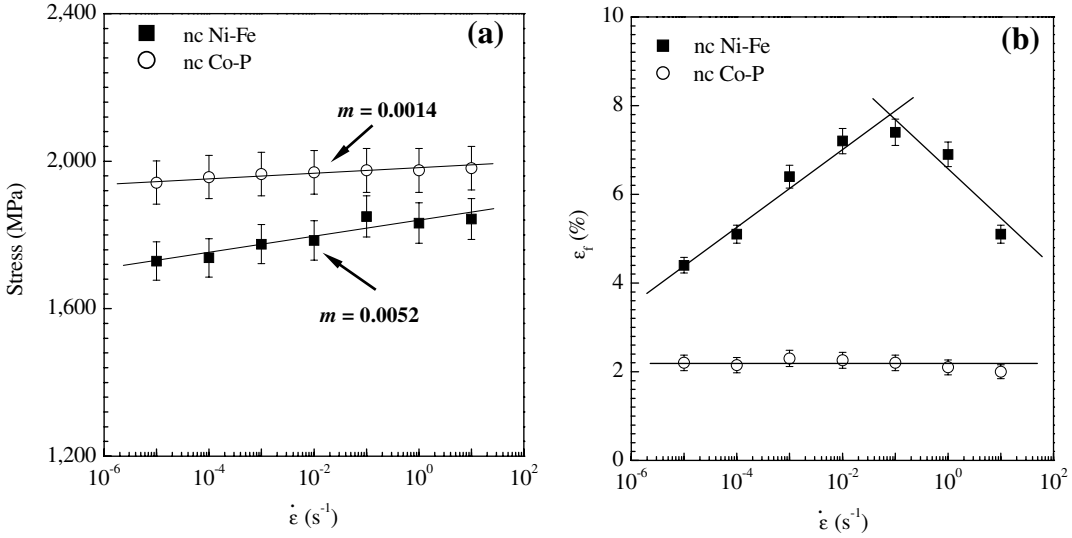

Fig. 7. The relationship (a) between the tensile stress at $\varepsilon = 2\%$ and the strain rates, $\dot{\varepsilon}$, indicates a very low strain rate sensitivity, m. The tensile elongation to failure, ε_f, as a function of $\dot{\varepsilon}$ for the bulk nc Ni–Fe and nc Co–P alloys is shown in (b). The straight lines in (a) were obtained from the best fit using Eq. (1); the straight lines in (b) were used as guides to the eyes.

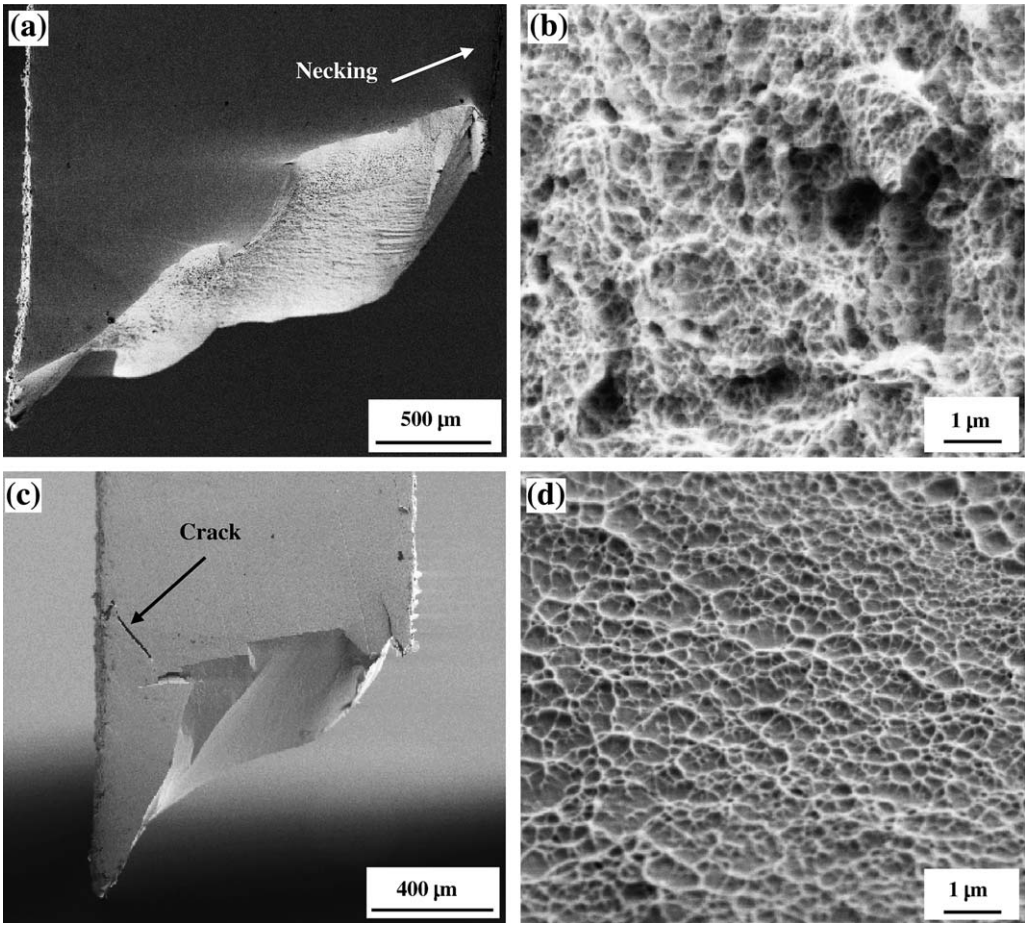

Fig. 8. SEM images of the fracture surfaces for the bulk nc Ni–Fe alloy deformed at $\dot{\varepsilon} = 10^{-3}$ s^{-1} to $\varepsilon_f = 6.4\%$ at a low magnification (a) and at a high magnification (b). SEM images of the fracture surfaces for the bulk nc Co–P alloy deformed at $\dot{\varepsilon} = 10^{-3}$ s^{-1} to $\varepsilon_f = 2.3\%$ at a low magnification (c) and at a high magnification (d).

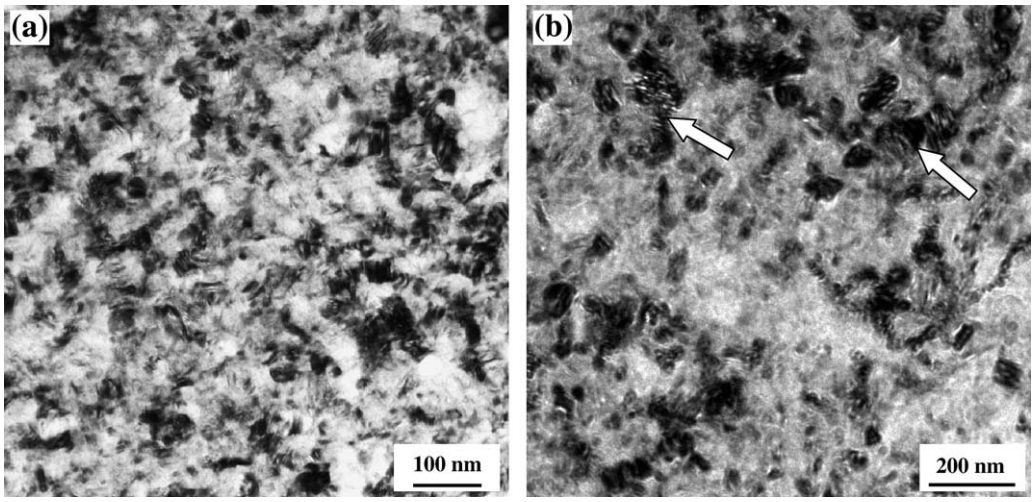

Fig. 9. Bright-field TEM images of the bulk nc Ni–Fe alloy after plastic deformation at $\dot{\varepsilon} = 10^{-3}$ s^{-1} to $\varepsilon_f = 4.0\%$ (a), and to $\varepsilon_f = 6.4\%$ (b). The images are perpendicular to the deposition growth direction. The images show the grain growth during the tensile deformation, compared to the average grain size of about 23 nm in the as-deposited state (Fig. 2). The arrows in (b) point to the large grains that underwent abnormal grain growth.

growth, a high volume fraction of grains larger than 200 nm was observed in the deformed specimens, leading to a bimodal distribution of the grain sizes.

The average grain size, d, of the nc Ni–Fe alloy after the tensile tests at various values of $\dot{\varepsilon}$ is plotted in Fig. 11(a). The d values increase with increasing $\dot{\varepsilon}$ from 10^{-5} to 10^{-2} s^{-1}, and decrease with further increasing $\dot{\varepsilon}$ to 10 s^{-1}. Since ε_f depends on $\dot{\varepsilon}$ (as shown in Fig. 7(b)), the relationship between d and ε_f is plotted in Fig. 11(b). It clearly shows that d increases with increasing ε_f.

The grain growth caused by the plastic deformation was also observed in the nc Co–P alloy. Fig. 12 shows a bright-field TEM image of the nc Co–P alloy deformed at $\dot{\varepsilon} = 10^{-3}$ s^{-1} to $\varepsilon_f = 2.3\%$. The grain size increased from approximately 12 nm in the as-deposited state (Fig. 3) to about 25 nm in the deformed specimen. In this case, the abnormal grain growth was not observed.

4. Discussion

Extensive experimental work has been performed previously to investigate the mechanical behavior of bulk UFG metals and alloys with average grain sizes in the range 100–1000 nm prepared by severe plastic deformation, such as equal-channel angular pressing (ECAP) and cold rolling [5–7,19,29–33,55–58]. These studies have provided

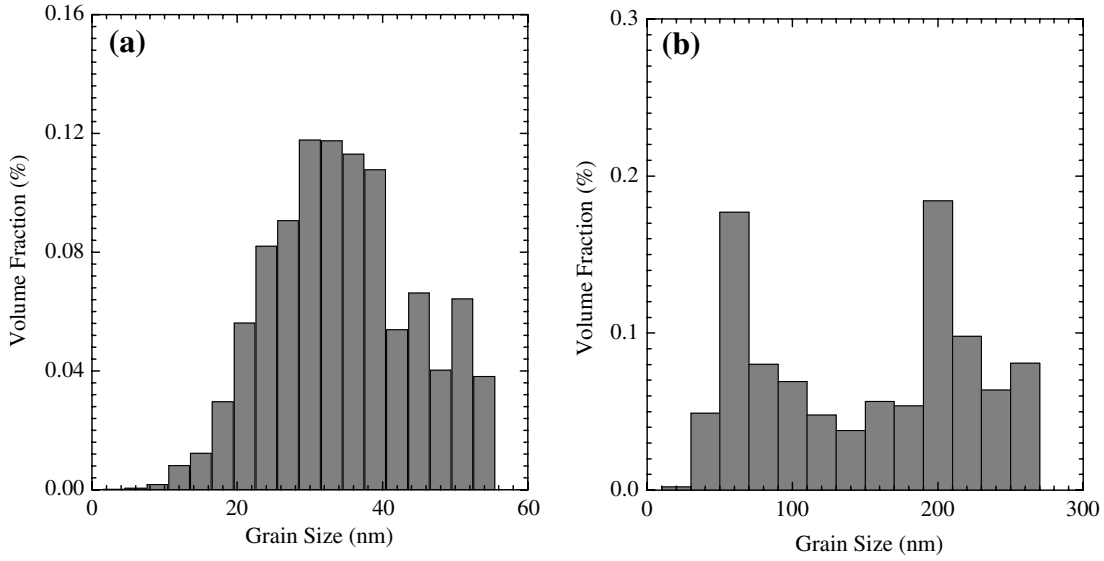

Fig. 10. Grain-size-distribution statistics of the bulk nc Ni–Fe alloy in the as-deposited state (a) and after the plastic deformation at $\dot{\varepsilon} = 10^{-3}$ s^{-1} to $\varepsilon_f = 6.4\%$ (b). A significant grain growth was observed after the plastic deformation. Moreover, a large volume fraction of large grains (i.e., $d > 200$ nm) suggests the occurrence of the abnormal grain growth.

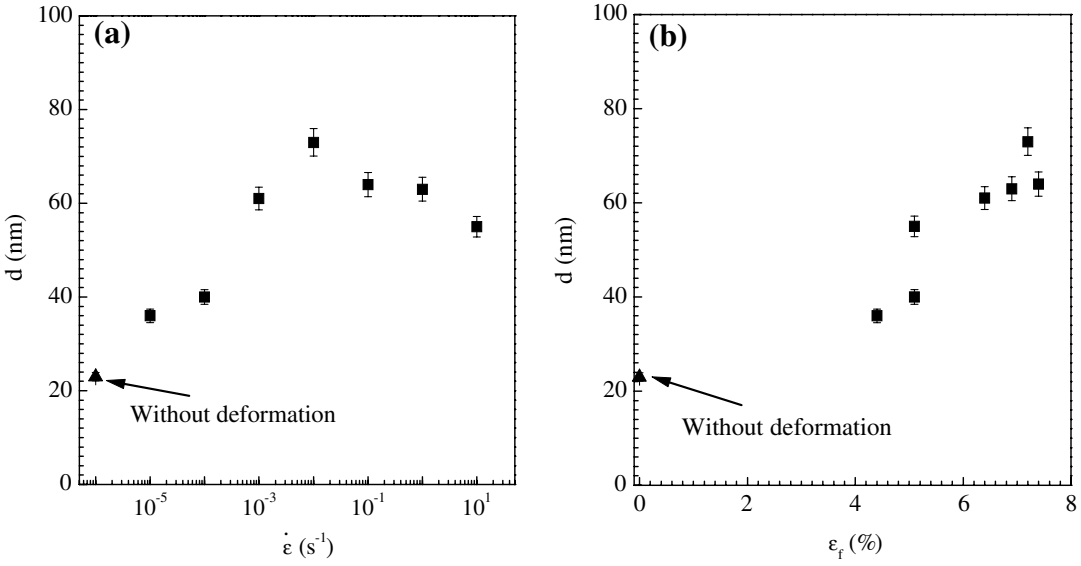

Fig. 11. Average grain sizes, d, of the bulk nc Ni–Fe alloy after the tensile plastic deformation at various strain rates, $\dot{\varepsilon}$ (a). Since the tensile elongation to failure, ε_f, of the specimen also depends on $\dot{\varepsilon}$ (Fig. 7(b)), the corresponding relationship between d and ε_f is plotted in (b). The d values increase with increasing ε_f.

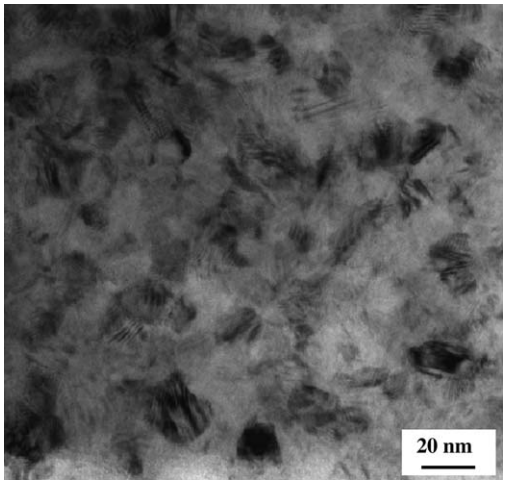

Fig. 12. Bright-field TEM image of the bulk nc Co–P alloy after the tensile deformation at $\dot{\varepsilon} = 10^{-3}$ s^{-1} to $\varepsilon_f = 2.3\%$. The image is perpendicular to the deposition growth direction. The grain size was increased from approximately 12 nm in the as-deposited state (Fig. 3) to about 25 nm after the tensile deformation.

the scientific and technological foundations for the potential engineering applications of these advanced materials. However, investigations of the mechanical properties and the deformation mechanisms of nc metals and alloys with average grain sizes in the range 2–100 nm were primarily focused on thin-film specimens [8,9,14,20,28,47–50], and were limited in the case of bulk specimens, due to the lack of tensile ductility with increasing specimen dimensions up to millimeters. In the following, we discuss several key issues related to the current experimental observations of the mechanical behaviors of the bulk nc Ni–Fe and nc Co–P alloys with average grain sizes less than 30 nm during uniaxial tensile tests at various strain rates.

4.1. Strength and ductility with varying strain rates

The study of the strain rate effects on the plastic flow of nc metals and alloys is important to understand their deformation mechanisms. For example, GB-mediated plasticity was suggested to be mainly responsible for the plastic deformation of nc metals and alloys. The GB-mediated plasticity, i.e., GB sliding accommodated by GB diffusion, requires a large value (i.e., >0.5) of the strain rate sensitivity, m [13,59]. Although the previous experimental results have indicated that the m value increases with decreasing grain size, the reported m values of nc metals were in the range 0.01–0.04, which is still too small to account for the GB-mediated plastic deformation [14,28,60,61]. Recently, several theoretical models have been proposed to explain the strain rate sensitivity of nc metals [28,62,63]. For example, Schwaiger et al. proposed that the GB-affected zone (GBAZ) accounts for the rate-controlled plastic deformation of nc metals [28]. On the other hand, Asaro and Suresh modeled the rate effects on the plastic flow of nc metals from the viewpoint of the various competing deformation mechanisms, including the emission of perfect and partial dislocation from GBs and from the twin boundaries [62].

In order to accommodate the different experimental setups at low strain rates and high strain rates (i.e., $>10^2$ s^{-1}), different sample geometries and dimensions were employed previously to measure the m values of nc metals. Since the mechanical properties of nc metals often show size effects, various experimental artifacts may mask the intrinsic m values of nc materials. In the present case, however, the

single geometry of the dog-bone bulk specimen was employed to study the mechanical properties of nc Ni–Fe and nc Co–P alloys at various $\dot{\varepsilon}$. The strength of both alloys shows a very weak strain rate dependence, yielding m values of 0.0052 and 0.0014 for nc Ni–Fe and nc Co–P alloys, respectively, which are one order of magnitude smaller than those for nc pure metals reported previously [14,28,60,61]. The very low m values of the current nc alloys may be due to the reduced GB mobility by the solution atoms such as Fe and P and/or to stress-induced grain growth (see Section 4.2). Soer et al. reported that the solute atom Mg effectively pins the high-angle GB mobility during in situ nanoindentation measurements in an Al–Mg film with grain sizes of the order of several hundred nanometers [38]. Nevertheless, as discussed below, the significant grain growth observed during the tensile plastic deformation indicates that GB activities indeed occur in these nc alloys.

It was previously reported that the tensile ductility of nc metals was sensitive to the change of $\dot{\varepsilon}$ [14,28,60,61]. Both the increase and the decrease of the tensile ductility with increasing $\dot{\varepsilon}$ were reported in the literature. Our study (Fig. 7) indicates that the tensile ductility of the nc Co–P alloy did not show a clear strain rate sensitivity, whereas the tensile ductility of the nc Ni–Fe alloy exhibits a strong strain rate effect, which peaks at a strain rate of about $10^{-1}\,s^{-1}$. By employing the concept of the GBAZ, the strain rate dependence of the tensile ductility of nc metals was theoretically analyzed by Schwaiger et al., suggesting that ε_f of nc Cu increases with increasing $\dot{\varepsilon}$ [28]. Apparently, this model cannot explain the reduced ε_f with increasing $\dot{\varepsilon}$ from 10^{-1} to $10\,s^{-1}$ for the present nc Ni–Fe alloy. It is suggested that the reduced ε_f at high $\dot{\varepsilon}$ value of the nc Ni–Fe alloy might be due to the lack of strain rate hardening effect, which results in the early necking instability, and eventual fracture of the samples during the tensile tests at high $\dot{\varepsilon}$ value.

4.2. Deformation-induced grain growth and its implications

Previous reports have indicated that a substantial grain growth may occur during in situ straining TEM observations in very thin nc Ni specimens [20], and during indentation experiments in nc and UFG metals at room temperature and even at a cryogenic temperature [38,46]. However, previous reports also indicated that the deformation-induced grain growth was significantly retarded with the addition of alloying impurity elements to pure metals, possibly because the impurity elements may segregate at the GBs, pin the GB migration and change the GB structure [38,41]. Only a small amount of grain growth was reported after alloying with impurity elements [38,41]. The current results presented in Figs. 9–12 clearly demonstrated that a substantial grain growth occurred during the tensile plastic deformation of bulk nc Ni–Fe and nc Co–P alloys, although the amounts of the grain growth seem to be somewhat smaller than that observed in the pure metals. The relationships among the average grain size, d, the strain rate, $\dot{\varepsilon}$, and the tensile elongation to failure, ε_f, in Fig. 11 indicate that the observed grain growth was caused by the plastic deformation. However, the previously reported grain growth from in situ straining TEM observations has been more recently attributed to electron-beam irradiation, rather than to plastic deformation [64]. Our ex situ TEM work, as well as recent high-energy XRD (HEXRD) experiments [45,46], rules out this possibility since our TEM samples before and after plastic deformation were under the same irradiation conditions.

A statistical analysis (Fig. 10(b)) of the TEM images (i.e., Fig. 9(b)) indicated that the abnormal grain growth occurred during the tensile plastic deformation of the nc Ni–Fe alloy. The abnormal grain growth was frequently observed during the recrystallization of heavily deformed polycrystalline metals [65–67]. Theoretical modeling and computer simulations have suggested that the non-uniform GB mobility may account for the abnormal grain growth caused by the thermal activation [67]. The reasons that the grains grow abnormally during the tensile plastic deformation of the nc Ni–Fe alloy at ambient temperature are not clear at the present stage. In addition to the non-uniform GB mobility, the possible existence of a local inhomogeneous stress distribution in the nc Ni–Fe specimen may also contribute to the observed abnormal grain growth. However, the exact mechanism by which the grains grow abnormally during the plastic deformation of nc metals and alloys is a subject for further investigations.

The grain growth occurring during the tensile plastic deformation of the nc Ni–Fe and Co–P alloys has two implications for their mechanical properties. First, the grain growth in the nc Ni–Fe and nc Co–P alloys may increase their tensile ductility, since the tensile ductility of nc materials often increases with increasing grain size. In the case of the nc Ni–Fe alloy, the abnormal grain growth during the tensile tests formed a bimodal microstructure (Fig. 9(b) and Fig. 10(b)), which will contribute to an additional tensile ductility, as reported previously in the literature showing a combination of high strength and good ductility in the bimodal UFG Al–Mg alloy and UFG/nc Cu metal [7,30–32]. Second, the simultaneous grain growth will cause the softening of the materials, resulting in the early necking of the samples. This necking process is further accelerated by the large localized plastic strain in the necking area, leading to a much more significant grain growth (up to several hundred nanometers) than the average amount of the grain growth in the uniform plastic deformation region [45]. The interplay between these conflicting effects will eventually influence the final tensile ductility of the nc metals and alloys. Compared with the nc Co–P alloy, the nc Ni–Fe alloy exhibits a large value of ε_f during the tensile tests. Based on the discussions presented above, the good tensile ductility of the nc Ni–Fe alloy can be attributed to (a) the lack of artifacts in the as-deposited state, which prevents the premature failure, and (b) the microstructure changes due to the spontaneous grain growth during the plastic deformation.

The strength of the nc alloys depends both on the strain rates and the average grain sizes. The effect of the strain rates on the strength of the nc materials was quantitatively evaluated by the m values (Eq. (1)). As shown in Fig. 11(a), the average grain sizes of the nc Ni–Fe alloy essentially increase with increasing strain rates, which will lead to strength reduction at high strain rates. Therefore, the interplay between the strength increase due to the strain rate increase and the strength decrease due to grain growth at high strain rates will eventually underestimate the intrinsic strain rate hardening effect, leading to a reduced m value, compared with nc materials without stress-induced grain growth.

The observed grain growth during the tensile plastic deformation of the nc Ni–Fe and nc Co–P alloys indicates that the plasticity of these nc materials is related to the GB activities, which is supported by the clear relationship between the average grain size, d, and ε_f of nc Ni–Fe as illustrated in Fig. 11(b). Molecular dynamics simulations have suggested that the grain growth might be due to: (a) GB migration leading to subgrain growth, and (b) grain rotation leading to subgrain agglomeration [68–70]. Recently, a HEXRD technique was employed to investigate the plastic deformation of an nc Ni–Fe alloy [45,46]. The quantitative HEXRD data confirmed that both the GB migration and grain rotation play roles in the observed grain coarsening.

Besides the GB activities involving GB migration and grain rotation, recent molecular dynamics simulations and experimental results suggest that mechanical twinning may be an important deformation mechanism for the nc materials, even for nc metals with high stacking fault energies, such as Al [10,11,15]. For the nc Ni–Fe alloy, growth twins were not observed in the as-deposited state. After the

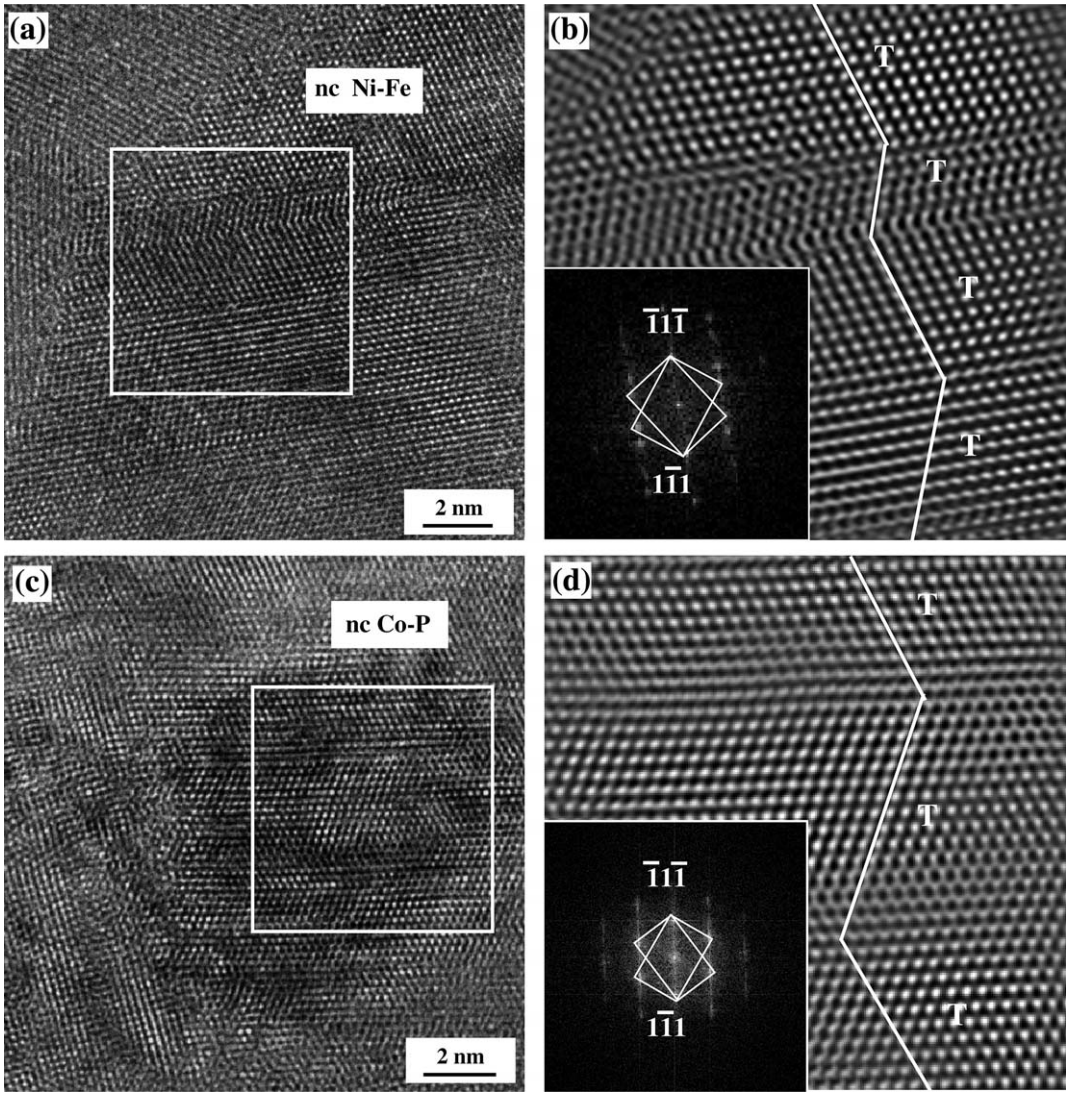

Fig. 13. HRTEM images (left) show the deformation twins in the bulk nc Ni–Fe alloy after the plastic deformation at $\dot{\varepsilon} = 10^{-3}$ s^{-1} to $\varepsilon_f = 6.4\%$ (a) and in the bulk nc Co–P alloy after plastic deformation at $\dot{\varepsilon} = 10^{-3}$ s^{-1} to $\varepsilon_f = 2.3\%$ (c). The inverse Fourier-filtered images (right) inside the white box in (a,c) show close-up views of the deformation twins (T) for the nc Ni–Fe (b) and nc Co–P (d) alloys. The fast Fourier transform (FFT) patterns in the inset of (c) and (d) indicate a $\Sigma 3$ $\{1\,1\,1\}$ twin boundary with a $[1\,1\,0]$ tilt axis for both nc alloys.

tensile plastic deformation, planar defects were sometime observed in the bright-field TEM images (not shown). These planar defects were identified to be deformation twins by HRTEM (Fig. 13(a)). A low density of the planar defects in the bright-field TEM images suggests that the twin density is low in the nc Ni–Fe alloy after tensile plastic deformation. In the case of the nc Co–P alloy, the as-deposited samples contained a large volume fraction of growth twins. After the plastic deformation, a high density of twins was frequently observable (Fig. 13(c)). The curvy part of the twin boundaries in Fig. 13 indicates that a high local stress field was built up in the twin boundaries. This high stress concentration is favorable for the formation of deformation twins. These results suggest that deformation twins may also play a role during the plastic deformation of nc Ni–Fe and nc Co–P alloys.

Finally, it is worth mentioning that dislocation activities may exist during the plastic deformation of the bulk nc Ni–Fe and Co–P alloys under investigation, as confirmed previously from in situ TEM observations of several nc metals [17–20,33,52]. The dislocation motions may play a dominant role during the plastic deformation in some nc materials, for example in nc Cu with average grain size about 10 nm as reported recently by Chen et al. [71].

5. Conclusions

The specimen size effects and strain rate effects on the tensile plastic flow of the bulk nc Ni–Fe and nc Co–P alloys, with average grain sizes of about 23 and 12 nm, respectively, have been investigated. A substantial grain growth was observed for both nc alloys after the tensile tests. Based on the experimental observations, the deformation mechanisms of the nc alloys have been discussed. From this study, it is concluded that:

1. The plastic flow of the bulk nc Ni–Fe alloy did not exhibit a clear specimen size effect, and the mechanical properties, including tensile ductility and fracture strength, remain almost constant when the sizes of the tensile specimens vary. However, the nc Co–P alloy showed a strong size effect, i.e., both the tensile ductility and the fracture strength decreased with increasing size of the tensile specimens. These results suggest that the nc Ni–Fe alloy was almost free of artifacts in the as-deposited state, as supported by a higher tensile elongation to failure during the tensile tests, in comparison to the nc Co–P alloy.
2. The strain rate sensitivity of both nc Ni–Fe and nc Co–P alloys is about one order of magnitude smaller that those reported for the pure metals, which can be attributed to the reduced GB mobility by the alloying elements. The tensile ductility of the nc Co–P alloy was not sensitive to the variation of the strain rates; in contrast, the tensile ductility of the nc Ni–Fe alloy showed a strong strain rate dependence.
3. A substantial grain growth was observed in both nc Ni–Fe and nc Co–P alloys after the tensile tests. The abnormal grain growth was observed in the nc Ni–Fe alloy, which may be due to the non-uniform GB mobility and/or to the local inhomogeneous stress distribution during the tensile tests. The abnormal grain growth led to a bimodal grain size distribution, which could contribute to the observed large tensile elongation to failure of the nc Ni–Fe alloy.
4. The dislocation motion and deformation twinning may still play roles in the plastic deformation of the nc Ni–Fe and nc Co–P alloys in combination with the GB activities.

Acknowledgements

G.J.F., H.C. and P.K.L. acknowledge the financial support from the National Science Foundation (NSF): (1) the International Materials Institutes (IMI) Program (DMR-0231320), (2) the Integration Graduate Education and Research Training (IGERT) Program (DGE-9987548), (3) the Combined Research and Curriculum Development (CRCD) Program (EEC-0203415) and (4) the Major Research Instrumentation (MRI) Program (DMR-0421219) with Dr. C. Huber, Dr. C.J. van Hartesveldt, Ms. M. Poats and C.R. Bouldin as program directors, respectively. The microscopy was performed at the National Center for Electron Microscopy, Lawrence Berkeley National Laboratory, supported by the Director, Office of Science, of the US Department of Energy (DoE) under Contract No. DE-AC02-05CH11231 and Grant No. DE-FG02-03ER46057.

References

[1] Koch CC, Morris DG, Lu K, Inoue A. Mater Res Soc Bull 1999;24:54.
[2] Nieman GW, Weertman JR, Siegel RW. J Mater Res 1991;6:1012.
[3] Weertman JR, Farkas D, Hemker K, Kung H, Mayo M, Mitra R, et al. Mater Res Soc Bull 1999;24:44.
[4] Sanders PG, Eastman JA, Weertman JR. Acta Mater 1997;45:4019.
[5] Valiev RZ, Islamgaliev RK, Alexandrov IV. Prog Mater Sci 2000;45:103.
[6] Valiev RZ, Alexandrov IV, Zhu YT, Lowe TC. J Mater Res 2002;17:5.
[7] Wang YM, Chen MW, Zhou FH, Ma E. Nature 2002;419:912.
[8] Kumar KS, Van Swygenhoven H, Suresh S. Acta Mater 2003;51:5743.
[9] Schuh CA, Nieh TG, Iwasaki H. Acta Mater 2003;51:431.
[10] Liao XZ, Zhao YH, Srinivasan SG, Zhu YT, Valiev RZ, Gunderov DV. Appl Phys Lett 2004;84:592.
[11] Yamakov V, Wolf D, Phillpot SR, Gleiter H. Acta Mater 2002;50:5005.
[12] Nieh TG, Wadsworth J. Scripta Metall Mater 1991;25:955.
[13] Fan GJ, Choo H, Liaw PK, Lavernia EJ. Metall Mater Trans A 2005;35:2641.
[14] Dalla Torre F, Van Swygenhoven H, Victoria M. Acta Mater 2002;50:3957.
[15] Chen MW, Ma E, Hemker KJ, Sheng HW, Wang YM, Cheng XM. Science 2003;300:1275.

[16] Hasnaoui A, Van Swygenhoven H, Derlet PM. Science 2003;300:1550.
[17] Hugo RC, Kung H, Weertman JR, Mitra R, Knapp JA, Follstaedt DM. Acta Mater 2003;51:1937.
[18] Mitra R, Chiou WA, Weertman JR. J Mater Res 2004;19:1029.
[19] Youssef KM, Scattergood RO, Murty KL, Koch CC. Appl Phys Lett 2004;85:929.
[20] Shan ZW, Stach EA, Wiezorek JMK, Knapp JA, Follstaedt DM, Mao SX. Science 2004;305:654.
[21] Schiotz J, Di Tolla FD, Jacobsen KW. Nature 1998;391:561.
[22] Froseth AG, Derlet PM, Van Swygenhoven H. Appl Phys Lett 2004;85:5863.
[23] Hasnaoui A, Derlet PM, Van Swygenhoven H. Acta Mater 2004;52:2251.
[24] Van Swygenhoven H, Derlet PM, Froseth AG. Nature Mater 2004;3:399.
[25] Budrovic Z, Van Swygenhoven H, Derlet PM, Van Petgem S, Schmitt B. Science 2004;304:273.
[26] Ke M, Hackney SA, Milligan WW, Aifantis EC. Nanostruct Mater 1995;5:689.
[27] Ma E. Scripta Mater 2003;49:663.
[28] Schwaiger R, Moser B, Dao M, Chollacoop N, Suresh S. Acta Mater 2002;50:3957.
[29] Koch CC, Youssef KM, Scattergood RO, Murty KL. Adv Eng Mater 2005;7:787.
[30] Tellkamp VL, Melmed A, Lavernia EJ. Metall Mater Trans 2001;32A:2335.
[31] Fan GJ, Wang GY, Choo H, Liaw PK, Park YS, Han BQ, et al. Scripta Mater 2005;52:929.
[32] Fan GJ, Choo H, Liaw PK, Lavernia EJ. Acta Mater 2006;54:1759.
[33] Youssef KM, Scattergood RO, Murty KL, Horton JA, Koch CC. Appl Phys Lett 2005;87:091904.
[34] Li HQ, Ebrahimi F. Appl Phys Lett 2004;84:4307.
[35] Li HQ, Ebrahimi F. Appl Phys Lett 2004;85:3749.
[36] Gu C, Lian J, Jiang Z. Adv Eng Mater 2006;8:252.
[37] Gleiter H. Acta Mater 2000;48:1.
[38] Soer WA, De Hosson JTM, Minor AM, Morris JW, Stach EA. Acta Mater 2004;52:5783.
[39] Zhang K, Weertman JR, Eastman JA. Appl Phys Lett 2004;85:5197.
[40] Jin M, Minor AM, Stach EA, Morris JW. Acta Mater 2004;52:5381.
[41] Zhang K, Weertman JR, Eastman JA. Appl Phys Lett 2005;87:061921.
[42] Liao XZ, Kilmametov AR, Valiev RZ, Gao HS, Li XD, Mukherjee AK, et al. Appl Phys Lett 2006;88:021909.
[43] Fan GJ, Fu LF, Qiao DC, Choo H, Liaw PK, Browning ND. Scripta Mater 2006;54:2137.
[44] Gianola DS, Petegem SV, Legros M, Brandstetter S, Van Swygenhoven H, Hemker KJ. Acta Mater 2006;54:2253.
[45] Fan GJ, Fu LF, Wang YD, Ren Y, Choo H, Liaw PK, Wang GY, Browning ND. Appl Phys Lett [in press].
[46] Fan GJ, Wang YD, Fu LF, Choo H, Liaw PK, Ren Y, et al. Appl Phys Lett 2006;88:171914.
[47] Karimpoor AA, Erb U, Aust KT, Palumbo G. Scripta Mater 2003;49:651.
[48] Cheung C, Djuanda F, Erb U, Palumbo G. Scripta Mater 1995;5:513.
[49] Qin XY, Lee JS, Lee CS. J Mater Res 2002;17:991.
[50] Choi P, da Silva M, Klement U, Al-Kassab T, Kirchheim R. Acta Mater 2005;53:4473.
[51] Lu L, Schwaiger R, Shan ZW, Dao M, Lu K, Suresh S. Acta Mater 2005;53:2169.
[52] Wei Q, Kecskes L, Jiao T, Hartwig KT, Ramesh KT, Ma E. Acta Mater 2004;52:1859.
[53] Kumar KS, Suresh S, Chisholm MF, Horton JA, Wang P. Acta Mater 2003;51:387.
[54] Hasnaoui A, Van Sygenhoven H, Derlet PM. Science 2003;300:1550.
[55] Iwahashi Y, Horita Z, Nemoto M, Langdon TG. Acta Mater 1997;45:4733.
[56] Fukuda Y, Oh K, Furukawa M, Langdon TG. Acta Mater 2004;52:1387.
[57] Stoica GM, Liaw PK. JOM 2001;53:36.
[58] Agnew SR, Mehrotra P, Lillo TM, Stoica GM, Liaw PK. Acta Mater 2005;53:3135.
[59] Luthy H, White RA, Sherby OD. Mater Sci Eng A 1979;39:211.
[60] Lu L, Li SX, Lu K. Scripta Mater 2001;45:1163.
[61] Wang YM, Ma E. Appl Phys Lett 2003;83:3165.
[62] Asaro RJ, Suresh S. Acta Mater 2005;53:3369.
[63] Zhu B, Asaro RJ, Krysl P, Bailey R. Acta Mater 2005;53:4825.
[64] Chen MW, Yan XQ. Science 2005;308:356c.
[65] Lee SB, Yoon DY, Henry MF. Acta Mater 2000;48:3071.
[66] Rios PR, Gottstein G. Acta Mater 2001;49:2511.
[67] Holm EA, Miodownik MA, Rollett AD. Acta Mater 2003;51:2701.
[68] Schiotz J. Mater Sci Eng A 2004;375–377:975.
[69] Haslam AJ, Phillpot SR, Wolf D, Moldovan D, Gleiter H. Mater Sci Eng A 2001;318:293.
[70] Moldovan D, Yamakov V, Wolf D, Phillpot SR. Phys Rev Lett 2002;89:206101.
[71] Chen J, Lu L, Lu K. Scripta Mater 2006;54:1913.